Polymer 49 (2008) 4680–4686

Contents lists available at ScienceDirect

Polymer

journal homepage: www.elsevier.com/locate/polymer

Effect of multi-walled carbon nanotubes on the lamellae morphology of polyamide-6

Anne-Carine Brosse [a], Sylvie Tencé-Girault [a,*], Patrick M. Piccione [b], Ludwik Leibler [a]

[a] Matière Molle et Chimie (ESPCI-CNRS, UMR 7167), ESPCI, 10 rue Vauquelin, 75231 Paris Cedex 05, France
[b] ARKEMA, Groupement de Recherches de Lacq, B.P. 34, RN 117, 64170 Lacq, France

ARTICLE INFO

Article history:
Received 14 April 2008
Received in revised form 31 July 2008
Accepted 4 August 2008
Available online 9 August 2008

Keywords:
Polyamide-6
Carbon nanotubes
Trans-crystalline lamellae

ABSTRACT

We show that crystal organization on both micro and nanoscales can be profoundly modified by dispersing carbon nanotubes (CNTs) in polyamide-6 by melt compounding. X-ray diffraction and transmission and scanning electron microscopies all indicate that when CNTs are well dispersed, crystalline spherulites are not present and remarkably crystalline lamellae grow aligning perpendicularly to the surface of the nanotubes. Such an epitaxial growth induced by CNTs during melt processing is particular to polyamide-6 because of crystallographic matching of CNTs and polyamide-6 crystal lattices. Macroscopically this epitaxial nucleation and growth can be detected and quantified by examining the splitting of the exothermic peak in calorimetric (DSC) experiments. Using optical microscopy and image analysis we show that the amount of *trans*-crystalline epitaxial crystallites increases when CNTs' dispersion quality is improved.

1. Introduction

Nanocomposites have been greatly developed during the last two decades to improve the electrical, mechanical and thermal properties of polymer materials. Carbon nanotubes (CNTs) are highly attractive fillers because of their high aspect ratio, their nanometer scale diameter, their mechanical strength and their electrical properties. When dispersed in various polymer matrices CNTs enable conductivity with a low percolation level. This improvement of electrical conductivity is sometimes even combined with a substantial improvement in mechanical properties [1–3]. To achieve these combinations of properties, the main challenge seems to have a proper dispersion of the CNTs in the matrix and a proper adhesion to the polymer matrix. Different methods have been reported for the preparation of CNT/polymer composites: solution processing [4,5], melt compounding [6–9] or in situ polymerization [10,11].

Polyamide-6 (PA-6) is a typical semi-crystalline thermoplastic polymer with a wide range of engineering applications, and not surprisingly literature on the dispersion of CNTs in this matrix is extensive [6,7,10,12–14]. Considerable effort has been devoted in particular to understand the modifications of the polyamide-6 crystallization by CNTs [12–14]. The key finding from these studies is the role of nanotubes as strong nucleation sites. Li et al. [12,14] showed that the MWNTs in the composite prepared by melt compounding accelerate the crystallization of PA-6. Moreover, the crystalline evolution is not the same in the composites and in the neat polyamide-6 depending on the cooling procedure. For neat polyamide-6, the crystallinity decreases when the cooling rate increases, while conversely, the crystallinity increases with cooling rate for the composite with 1 wt% [14]. After a quench, the composites end up with a higher degree of crystallinity than the neat polyamide-6. For pristine MWNT composites prepared by melt compounding, Li et al. [14] and Phang et al. [13] showed by WAXS that the only crystalline form present is the α form without change in the cell parameters or in the melting temperature and this is independent of the cooling rates. Moreover, Phang et al. [13] observed that the temperature of crystallization is split into two peaks, Tc1 and Tc2. However, not all the studies on the crystallization of CNT/PA-6 composites [12,14] show such a splitting and its significance is not well understood.

The question of the exact influence and of the control of CNTs on the crystallization is still open. Here, we combine careful quantitative studies of the quality of CNTs' dispersions and crystallization of PA-6 matrix and show, for the first time, that when CNTs are well dispersed, the spherulite structure is absent and PA-6 crystalline lamellae grow from the CNTs surfaces and align perpendicular to them. This epitaxial growth is possible thanks to the lattice matching between the CNTs and the PA-6 crystals.

The crystallization morphology of the matrix is important for the mechanical properties; it may affect properties such as

* Corresponding author. Tel.: +33 (0)1 40 79 51 24; fax: +33 (0)1 40 79 51 17.
E-mail address: sylvie.girault@espci.fr (S. Tencé-Girault).

0032-3861/$ – see front matter © 2008 Elsevier Ltd. All rights reserved.
doi:10.1016/j.polymer.2008.08.003

strength, hardness and toughness [15–17]. The crystallization is affected by the processing conditions which include, among other things, shear flow, addition of fillers, temperature of the melt and kinetics of cooling. All types of fillers or nanofillers, rigid or soft can strongly influence the crystallization of the matrix. Corte et al. [18] showed that differences in the crystalline organization of the polyamide-12 matrix can induce dramatic changes in the toughening efficiency of polyamide-12/rubber composites. *Trans*-crystalline regions have been observed in the vicinity of soft [19] and rigid [20] nanofillers in PA-6; these *trans*-crystalline layers are made up of periodic crystalline lamellae perpendicular to the nanofiller/polymer interfaces. Dasari et al. [20] showed that these *trans*-crystalline layers exist only in the core region of injected-molded PA-6 and not in the surface region where the flow-induced crystallization mechanism dominates. For clays, the influence of *trans*-crystalline layers on the mechanical properties was modeled by Sheng et al. [21]. For nylon-6/clay nanocomposites, using finite elements simulation techniques, they assumed that each particle has a *trans*-crystalline matrix layer on either side and they found that this effect is minor in comparison with the "composite level" effect.

To understand better this important issue of the influence of CNTs on crystallization, we study the modifications of the crystalline organization induced by carbon nanotubes in polyamide-6 composites for controlled and quantified state of dispersion. With the help of transmission electron microscopy observations of composites, we show the existence of periodic *trans*-crystalline lamellae of PA-6 on the nanotube surface. *Trans*-crystalline lamellae have been observed in many semi-crystalline polymer composites with various fillers and various matrices [22]. Shi et al. [23] observed the *trans*-crystalline lamellae in polyamide-6 induced by the dispersion of Kevlar fibres in films cooled from the melt. WAXS studies enabled Kojima et al. [24] to show that the molecular chains are parallel to the montmorillonite platelets. Similar conclusion has been reached from transmission electron microscopy (TEM) in polyamide-12 by Kim et al. [25]. For CNTs, *trans*-crystalline lamellae growing perpendicular to nanotube surfaces have been observed, by scanning electron microscopy (SEM) for PP [26] and deduced from WAXS analysis for PE [27]. More recently, Li et al. [28,29] reported the formation of another interesting structure in the presence of carbon nanotubes, which they called nanohybrid shish–kebab, where the CNTs formed the shish and the nylon-66 [28] or the PE [29] formed the "kebab". However, structures were obtained at 185 °C by solution crystallization and that they cannot be compared to *trans*-crystalline lamellae observed here by melt process.

In this work, we present the crystalline modifications induced by carbon nanotubes in polyamide-6. All our observations were made at a controlled state of dispersion of nanotubes. Microscopic observations show the disappearance of PA-6 spherulites whereas nanoscopic observations prove the existence of the *trans*-crystalline layer. We also observe the splitting of the crystallization peak and associate the high endothermic peak to the crystallization of the *trans*-crystalline layer. We believe this *trans*-crystalline layer to be an epitaxial growth of PA-6 crystal on nanotube surfaces at high temperatures.

2. Experimental section

2.1. Materials

Polyamide-6 (BASF, Ultramid® B3) was dried before use at 80 °C for 12 h and used as pellet or powder. multi-walled carbon nanotubes (MWNTs) produced by catalytic chemical vapor deposition (CCVD) were provided by Arkema (Graphistrength™ C100) [30]. The MWNTs were purified by refluxing in sulfuric acid. Their mean diameter was 10 nm and their length ranged between 0.1 and 10 μm.

2.2. Sample preparation

PA-6 composites containing various amounts of MWNTs (0–10 wt%) were prepared by melt compounding using a DACA micro-extruder. This compounder is a 5 cm^3 capacity co-rotating twin-screw extruder with a feedback channel allowing cyclic extrusion, and adjustable mixing times. Polyamide and nanotubes were blended at 250 °C, under a N_2 atmosphere, at various rotation speeds, for 10 min. Samples were then air cooled. The samples were designated by PA*x*NT-*y* where "*x*" represents the load of the compound and "*y*" the speed rate of mixing in rpm.

2.3. Microscopy characterization

Optical transmission microscopy observations were performed on extruded rods. Sections between 5 and 3 μm in thickness (depending on the nanotube loading) were cut from the composites at ambient temperature on a Leica RM 2265 microtome. Three different cuts were obtained for each sample to check the dispersion homogeneity; the area explored is about 9 mm^2.

Scanning electron microscopy (SEM) measurements were performed using a FEG XL30 Philips microscope. The extruded samples were cryo-fractured using liquid nitrogen and sputtered with gold and palladium.

Transmission electron microscopy (TEM) observations of composites were performed with a CEM 902 Zeiss microscope operated under an acceleration voltage of 80 kV. Thin sections (60 nm) were cut from the composite after melt compounding under cryogenic conditions using a Leica Ultracut microtome with a diamond knife. The sections were stained by an aqueous solution of phosphotungstic acid ($H_3PO_4 \cdot 12WO_3$) and benzyl alcohol [31]. Benzyl alcohol helps diffusion of WO_3 in amorphous polyamide layers, so the crystalline lamellae of polyamide matrix are revealed. For the spherulite observations, the sections were stained by OsO_4.

2.4. Differential scanning calorimetry

A TA Instrument DSC Q1000 differential scanning calorimeter (DSC) was used to study the crystallization and the melting of the composites. The first heating from 20 to 260 °C at 10 °C/min was recorded then the samples were maintained at 260 °C for 5 min to delete any previous thermal history. The composites were then cooled at 10 °C/min from 260 °C to −100 °C under nitrogen atmosphere to analyze the crystallization.

2.5. X-ray diffraction experiments

The crystallization was characterized by Wide-Angle X-ray Scattering (WAXS) and Small-Angle X-ray Scattering (SAXS). X-ray scattering experiments were performed at room temperature in transmission mode using the Cu Kα radiation ($\lambda = 1.54$ Å) from an X-ray generator (XRG3D Inel) operating at 40 kV and 25 mA. WAXS patterns were collected with a curve position sensitive detector (CPS120 Inel) and were fitted using the Peakoc Inel Software for crystallinity calculations. SAXS curves were acquired with a linear detector (LPS50 Inel) 170 cm away from the sample. This allowed the observation of scattering intensities at q values from 0.006 to 0.09 $Å^{-1}$. Standard data corrections were applied for both SAXS and WAXS measurements; the spectra were normalized by the transmission and the thickness of the sample, the intensity of the incident beam, the acquisition duration and finally corrected for background scattering.

3. Results and discussion

3.1. Control of the state of dispersion

The focus of this work is the study of nanotube content on the morphology and crystallization of the polyamide-6 matrix, irrespective of the dispersion state. Therefore it is essential for us, to control this dispersion state.

The carbon nanotube dispersion state in a polymer matrix can be characterized at various scales, from the macro to the nano. The first and essential step to quantify this state is the macroscopic level accessible by optical microscopy. At this scale it is possible to detect and quantify the amount of micrometer size aggregates. If no aggregate is found at this scale, smaller length scales can be explored with other techniques, such as the electronic microscopies.

We optimized our compounding parameters by quantifying the level of dispersion by optical microscopy associated with image analysis. We prepared samples with the same loading of nanotubes but at different extruder screw speed rates. The transmission pictures obtained by optical microscopy were treated with the ImagJ software [32] to determine the proportion of surface covered by dark spots. The difference in dispersion state can be clearly seen from Fig. 1 for three different compounding conditions. The composite melt mixed at 50 rpm (Fig. 1a) shows large dark spots corresponding to nanotube aggregates, while the composite melt mixed at 200 rpm shows no aggregates at this scale (Fig. 1c). On each micrograph, we have also reported the quantification obtained with the image analysis (the proportion of dark surface), the differences are significant and in line with our subjective assessment of the level of dispersion.

We used this method to define our final compounding conditions: 250 °C, 200 rpm and 10 min; the results about temperature and time are not discussed here. At these conditions, we were able to prepare samples by melt mixing with different loads of CNTs from 0.1 to 10% showing no nanotube aggregates detected by optical microscopy.

3.2. Crystallization study

Well dispersed composites were then prepared with the amount of nanotubes ranging from 0.1 to 10%.

During the first heating, we observe only small change of the endothermic signal after the introduction of carbon nanotubes. Only one melting peak at 222 °C is present for the composite with CNTs or without CNTs. This endothermic peak corresponds to the α phase of the PA-6. The melting temperature of α phase does not change with the concentration of CNTs. The peak becomes broader because the size of the crystallites becomes more heterogeneous. No significant evolution with the concentration of nanotubes is present.

Non-isothermal crystallization from the melt was then studied with a cooling rate of 10 °C/min. Exotherms are presented in Fig. 2. We observe a significant evolution of the crystallization exotherm with the concentration of nanotubes. For the neat polyamide-6, the crystallization peak is sharp and its maximum is at 189 °C. For all the well dispersed CNT composites, this peak is broader, but also shifts to higher temperatures and splits into two components. By integration of the crystallization peak, we can estimate the crystallization enthalpy. After correction of the composition, a slight evolution of the enthalpy is observed as reported in Table 1, up to a 25% increase at 10 wt% of CNTs. If we index the peak at higher temperature as peak 2, at a temperature T_{C2} and with intensity from the base line I_2, and with index 1 the lower temperature peak, the evolution of I_2/I_1 can be determined and is reported in Table 1. The two peaks shift to higher temperatures at higher CNT contents. This effect is more pronounced for peak 2, and in addition, the relative proportion of peak 2 increases. Above 3–5%, peak 2 becomes the main peak and peak 1 becomes an additional peak (Fig. 2).

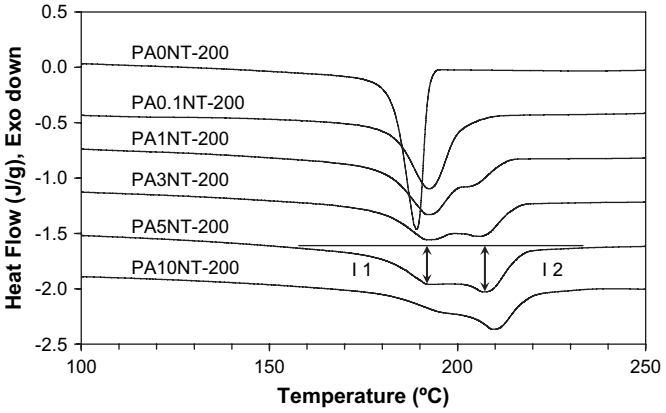

Fig. 2. DSC cooling curves of PA-6/MWNT composites at different MWNTs loadings.

Table 1
Crystallization temperatures (T_{C1} and T_{C2}) and intensity ratio (I_2/I_1), enthalpy (ΔH_C) and crystallinity ($\chi_{C\text{-}XRD}$) of PA-6/MWNT composites at different MWNT loadings

Sample	T_{C1} (°C)	T_{C2} (°C)	I_2/I_1	ΔH_C (J/g)	$\chi_{C\text{-}XRD}$ (%)
PA0NT	189.0			63	22
PA1NT-200	191.5	201	0.50	67	21
PA3NT-200	192.0	206	0.90	66	22
PA5NT-200	194.0	207	1.19	74	24
PA10NT-200	197.5	209	1.65	79	26

Fig. 3 presents the evolution of the crystallization peak for composites prepared with 1 wt% of nanotubes, but with various qualities of dispersion. Unlike the case when the CNTs' content changes, the temperatures of the two peaks T_{C1} and T_{C2} remain constant; only the relative intensity of the two peaks changes with the dispersion state. The intensity of peak 2 increases with the quality of the dispersion. We conclude that peak 2 is associated with the interface between polymer and CNTs and can be an indication of the dispersion state. We further assume that this crystallization peak is related to the crystalline lamellae which are

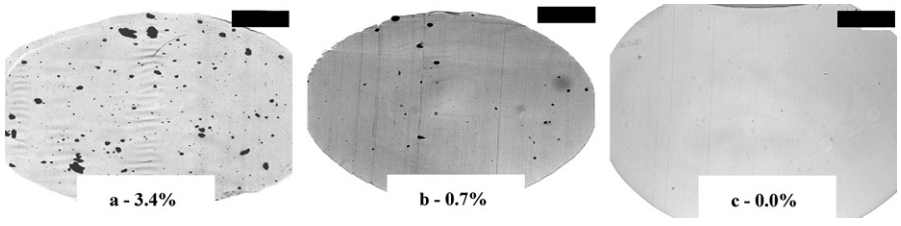

Fig. 1. Optical microscopy images of PA-6/MWNT composites with 1 wt% loading after melt mixing with the indication of the proportion of surface covered by dark spots – scale bar 400 μm – (a) PA1NT-50, (b) PA1NT-100, (c) PA1NT-200.

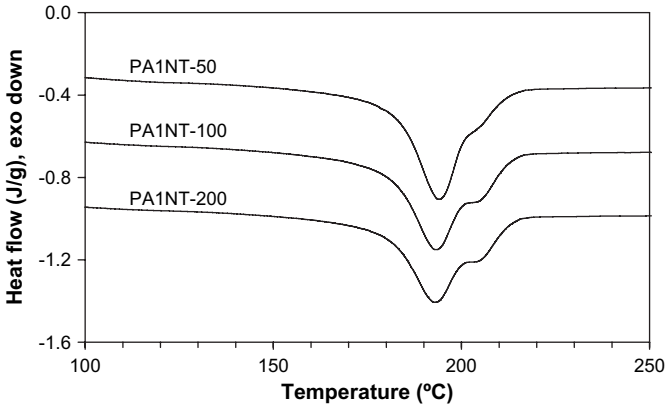

Fig. 3. DSC cooling curves of PA-6/MWNT composites with 1 wt%, and with various qualities of dispersion.

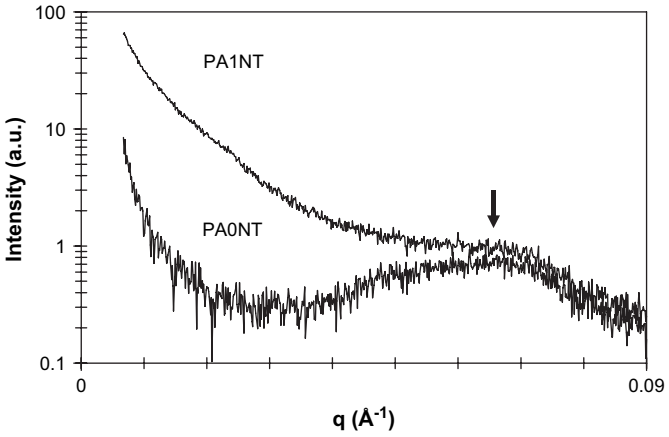

Fig. 5. SAXS patterns of neat PA-6 and PA-6/MWNT composites with 1 wt%.

nucleated by the CNTs whereas peak 1 is related to the crystalline lamellae which are not directly connected to CNTs' surfaces.

Phang et al. [13] observed this splitting of the crystallization peak in his composites, made with a Brabender at 100 rpm during 10 min, and concluded that the peak at higher temperature originates from chains tethered to the nucleation sites of MWNTs. This additional peak surprisingly has not always been observed in PA-6/CNT composites [12,14]. Li et al. [12,14] studied composites prepared by melt blending, with a Brabender twin-screw extruder at 30 rpm, with functionalized or non-functionalized MWNTs. They observed, with a cooling rate of 10 °C/min and a load of 1 wt%, an increase of the crystallization temperature of 3 °C, a broadening of the peak by a factor of 2 or 1.5, respectively, for the functionalized or non-functionalized MWNTs, but no splitting of the peak. We can wonder why only Phang et al. [13] noticed this phenomenon. Probably, as mentioned above the quality of dispersion can be put forward and perhaps the functionalization of nanotubes decreases this effect by disrupting the crystallization.

A possible mechanism for the existence of these two crystallization peaks observed for our samples could be the successive crystallization of two crystalline phases. To confirm this, we performed X-ray experiments on neat polyamide and its composites. The X-ray diffraction profiles of neat polyamide and of the well dispersed composite with 1 wt% of nanotubes are reported in Fig. 4; these profiles are representative for all the well dispersed composites at different loadings from 0 to 10 wt%.

They contain peaks at $2\theta = 20.2°$ and 23.8°, associated with the (200) and (002) reflections of the α crystalline phase of PA-6 [33]. The WAXS spectra were all fitted using a Peakoc Inel Software which uses Pseudo-Voigt profiles. The curve fits allow the

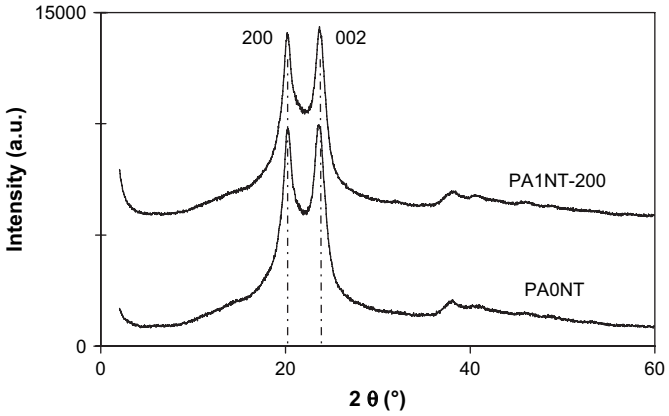

Fig. 4. WAXS patterns of neat PA-6 and PA-6/MWNT composites with 1 wt%.

decomposition of the scattering spectra into amorphous broad peaks and crystalline narrow peaks. From this decomposition, the crystallinity ratios for each composite can be calculated as the ratio between the total intensities of the crystalline peaks and the summed intensities of all peaks. This crystallinity ratio is corrected for the concentration of nanotubes to estimate the PA-6 crystallinity. These values ($\chi_{C\text{-}XRD}$), reported in Table 1, show only a slight increase, 18% for 10 wt% of nanotubes, comparable to the evolution of the crystallization enthalpy (ΔH_C). These X-ray observations are in agreement with those of Li and al. [14] for slowly cooled samples, but do not explain the evolution of the crystallization exotherm peak observed with DSC experiments.

We also performed SAXS experiments to explore a wide range of characteristic distances of the organization. Scattering intensity profiles from $q = 0.006$ to 0.09 Å^{-1} are plotted in Fig. 5. Around $q = 0.065$ Å^{-1}, the signal observed is associated with the crystalline and amorphous periodic lamellae organization of the polyamide. There is no modification of this periodic distance, estimated at $L_p = 92 \pm 5$ Å, whatever the concentration of MWNTs between 0 and 10 wt%. When nanotubes are incorporated in the polyamide, an important increase of the intensity is observed in the small angle area due to the diffusion of the carbon nanotube.

So, regardless of the MWNTs concentration (0 to 10 wt%), the crystalline structure and the periodic organization of crystalline and amorphous lamellae are not modified. To summarize no structural evolution can explain the evolution of the crystallization peak.

3.3. Morphological study

At the crystallographic scale explored by SAXS and WAXS measurements, there are no differences that can explain the presence of the second crystallization peak, so we investigated the lamellar organization. TEM pictures stained by OsO_4 and SEM pictures, in the inset, of the cryo-fractured surface of polyamide-6 and its composite with 0.1 wt% MWNTs are presented in Fig. 6. The dispersion seems correct since at this scale no aggregates are visible. For neat PA-6 (Fig. 6a), spherulites of 5 μm in diameter are visible. For the composites with 0.1 wt% of MWNTs (Fig. 6b), by contrast no spherulites or any "organization of the lamellae" can be seen at this scale. These observations are similar for the composites with higher loading (1, 3, 5 and 10 wt%) by SEM and optical microscopy. So no organization of the lamellae can be seen; the presence of these lamellae is detected by SAXS. We therefore explored the lamellae organization by TEM.

TEM images (Fig. 7) of the sections of polyamide-6 and composites after staining with phosphotungstic acid show the contrast between crystalline and amorphous lamellae of polyamide-6 crystalline

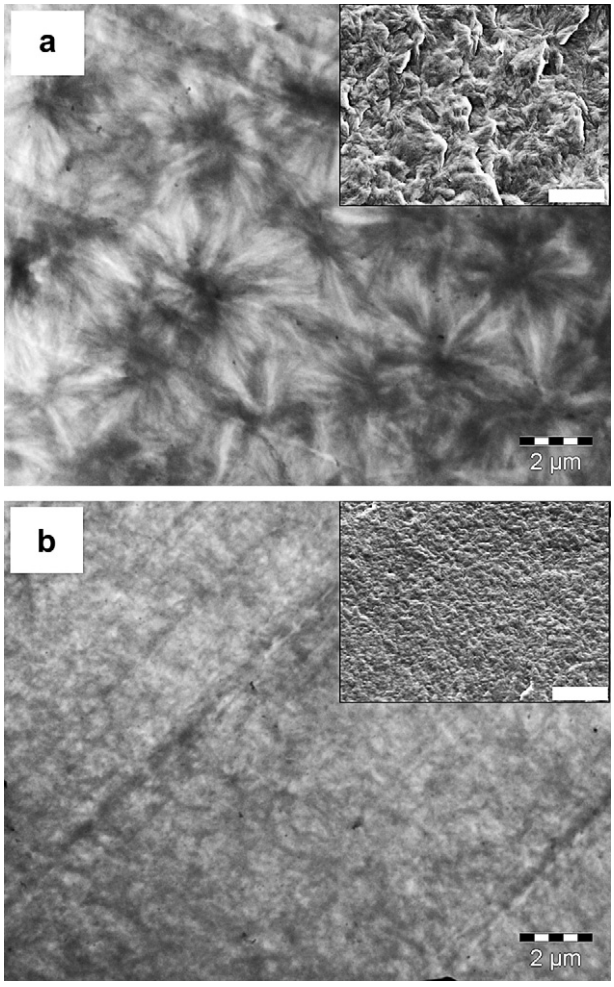

Fig. 6. TEM images of PA-6/MWNT composites with (a) 0 wt%, (b) 0.1 wt% and inset shows the SEM images of the same composites – scale bar 2 μm for TEM and 5 μm for SEM.

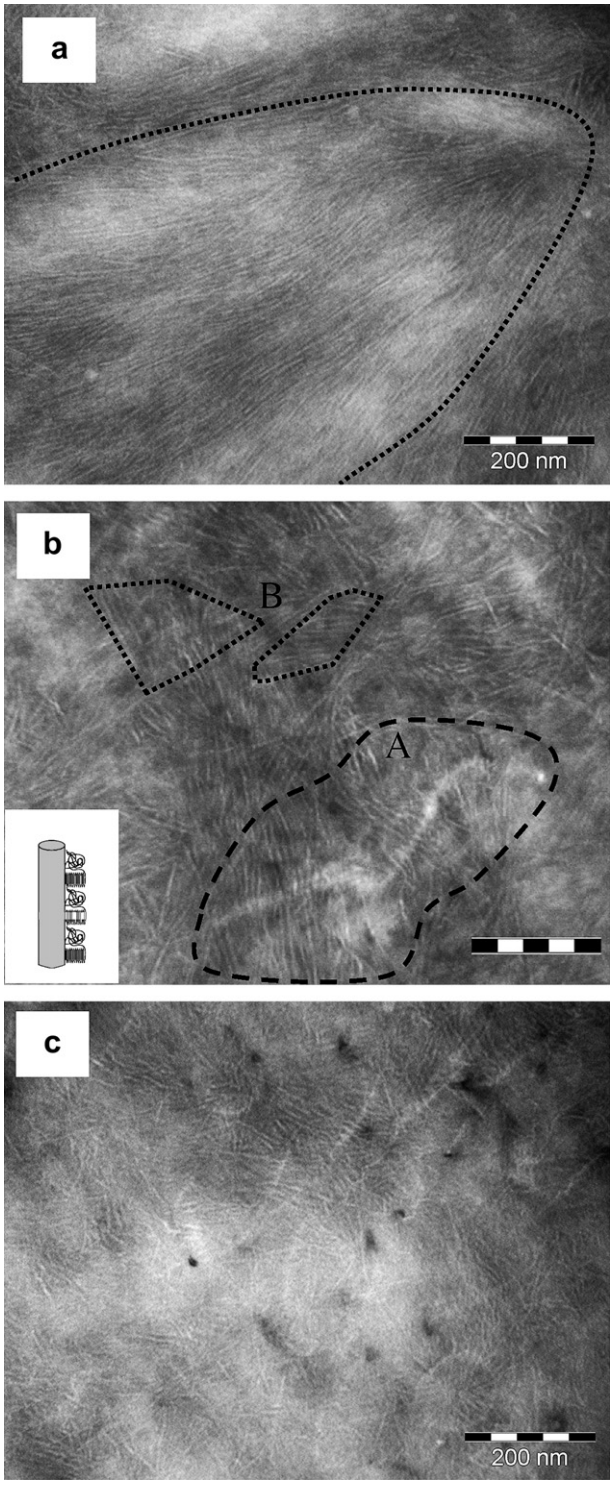

Fig. 7. TEM images of PA-6/MWNT composites with (a) 0 wt%, (b) 0.1 wt%, (c) 1 wt% – scale bar 200 nm.

organization. The phosphotungstic acid diffuses more quickly in the amorphous phase so this phase appears darker. For pure PA-6, lamellae of hundred of nanometres length are measured (Fig. 7a). The lamellae organization is correlated on scale of hundreds of nanometres. So important stacks of long lamellae can be seen, outlined by the line in black. For the composites with 0.1 wt% (Fig. 7b), there are two types of lamellae. *Trans*-crystalline lamellae are observed, with length of about 200 nm, forming a layer perpendicular to CNTs whatever the orientation of CNTs. The zone A on Fig. 7b circles one nanotube and its *trans*-crystalline layer, and the inset shows a schematic representation of lamellae on nanotube. A second type of lamellae is organised in short stacks of about 10 lamellae (defined by B in Fig. 7b) without any organization at long distance; these lamellae do not seem to grow from the CNTs. In this organization, no lamellae longer than 400 nm can be seen. When the load of CNTs increases, the lamellae morphology remains similar, but the length of the lamellae decreases, probably because the distance between CNTs decreases. At 1 wt% (Fig. 7c), the length of *trans*-crystalline layer is about 60 nm.

Trans-crystalline lamellae have already been mentioned in carbon nanotube composites based on other semi-crystalline polymers. Haggenmueller et al. [27] prepared composites of PE/SWNT by the hot coagulation method. By WAXS measurements, they observed that SWNT template PE crystallization in isotropic and oriented composites. The same orientation for the PE chain and the SWNT was attributed to the growth of crystalline lamellae perpendicular to the SWNT with chains parallel to the nanotubes. Sandler et al. [26] observed the presence of *trans*-crystalline lamellae by SEM in PP/MWNT composites prepared by solution casting, but no optical observation was realized. In PP [34] for films cooled from the melt state and PE [27] for films crystallized from solution, spherulites on micrometer scale were detected by optical microscopy, but for both these composites no TEM observations were carried out. So, the only direct observation (by SEM) of *trans*-crystalline lamellae was made after solution preparation.

For our PA-6/MWNT composites, no spherulites can be observed, after a slow cooling from the melt. We think that this lack of spherulites and the organization of the lamellae in stacks, in the matrix, without long range order, can be explained by a confined crystallization between the MWNTs. Indeed, even at only 0.1 wt% of well dispersed MWNTs, the distance between MWNTs is already less than 1 μm. The same estimation can be made with every polymer. But, if we attribute the higher crystallization peak, at T_{C2}, to the crystallization of the *trans*-crystalline lamellae from the surface of CNTs, when the crystallization of the free lamellae in the matrix begins, at T_{C1}, the growth of *trans*-crystalline lamellae is complete and the free volume is limited. The crystallization takes place in a confined space of about 0.5 μm. This situation persists as long as the surface of nanotubes creates a lot of high temperature nucleation centers. We want to point out that some authors [13] observed spherulites in their PA-6/MWNT composites by optical microscopy, although this can come from the preparation method. In fact in thin film melts, the CNTs can agglomerate so the crystallization mechanism may be different.

We have seen that PA-6 in composites crystallizes in the α phase (WAXS) with a periodic amorphous and crystalline lamellar organization. By SAXS experiments, we measure a period of 92 Å, and we measure the same distance between two successive lamellae perpendicular to nanotubes on TEM images. In this polyamide structure, chains are aligned along the $\vec{b}$ direction which is perpendicular to the folding surface of the lamellae. The orientation of lamellae perpendicular to the nanotubes means that the polymer chains themselves are in fact aligned along the axis of nanotubes. If we suppose epitaxial growth of polyamide crystals, there are two possible orientations for this growth with, the $(\vec{a}, \vec{b})$ or the $(\vec{b}, \vec{c})$ plane parallel to the surface of the nanotubes, corresponding, respectively, to the two orientations of Model a and Model b proposed in Fig. 8.

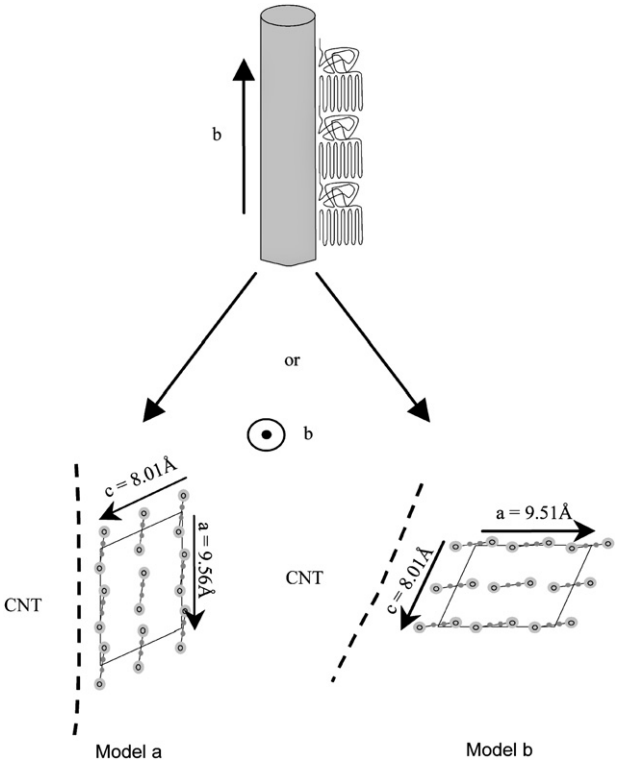

Fig. 8. Two orientations for the epitaxial growth of PA-6 lamellae with – Model a – the $(\vec{a}, \vec{b})$ plane on the nanotube surface and – Model b – the $(\vec{b}, \vec{c})$ plane on the nanotube surface.

Shi et al. [23] investigated the *trans*-crystalline morphology of nylon 6 induced by Kevlar fibres. To discriminate between different models of relative orientations, they compared the matching between the crystallographic lattice of the Kevlar fibres and the nylon 6 crystal. The mismatching can be defined as follows:

$$\Delta = 100 \times \frac{d - d_0}{d_0}\%$$

where d is a cell parameter of the polymer and d_0 is a cell parameter of the fibers' structure. Carbon nanotubes are graphene cylinders coaxially arranged so the structure of the surface of the nanotubes is a graphitic hexagonal lattice. Sano et al. [35] studied a model of epitaxial growth of the nylon 6 chain on a graphitic surface by STM. In their model, the polymer chains are parallel to the surface in an all-*trans* conformation, with adjacent chains being anti-parallel. Each amide group was placed on a relevant repeating unit of the graphite hexagonal lattice separated by 8.52 Å along the chain and by 4.92 Å between chains. In this case, the orientation of the epitaxial growth corresponds to the Model a where the $(\vec{a}, \vec{b})$ plane of PA-6 is parallel to the CNTs' surface. The mismatching is 1.2% for parameter b and 2.8% for parameter a, this value of Δ is small compared to the upper boundary of mismatch (15%). For the Model b with the $(\vec{b}, \vec{c})$ plane parallel to the surface of the nanotubes, the mismatching for the parameter c is 8.5%. It is larger than the mismatch for the parameter a. Moreover for the Model a, all the hydrogen bonds can be optimized which is not in the case of Model b when $(\vec{b}, \vec{c})$ planes are parallel to the CNTs' surface. The Model a seems more likely. So the growth of the nylon 6 *trans*-crystalline lamellae from the MWNTs can be attributed to a matching between the nylon 6 and the MWNT crystallographic lattice.

4. Conclusion

Our optical microscopy studies show that CNTs can be well dispersed in PA-6 by melt blending without using any particular dispersing aids. The MWNTs influence the crystalline morphology, leading to important modifications. The carbon nanotubes increase the crystallization temperature and if they are well dispersed, lead to a splitting of the crystallization peak with two characteristic temperatures. The crystallization peak, at higher temperature, is not due to a different crystalline phase, because only the alpha phase is present. The overall crystallinity is slightly increased and no changes in cell parameters or lamellae period are observed. The splitting was therefore assigned to morphological modifications. We did not observe spherulite organization but rather, two types of lamellae stacks, one for each peak of crystallization: lamellae independent of CNTs in the matrix and *trans*-crystalline lamellae that grow perpendicularly to the CNTs surfaces, with the polyamide chains parallel to the axis of the nanotubes.

For the first time, in PA-6 composites prepared by melt mixing, we show by TEM the presence of periodic *trans*-crystalline lamellae on the nanotube surfaces. This fact seems to be a particularity of PA-6, which has crystallographic lattice matching that of carbon nanotubes. This morphology should have important consequences on the mechanical or electrical properties of composites. The existence of this crystalline polymer layer around nanotubes should have an effect on the conductivity by creating an insulating layer around the CNTs, and can explain the difference of percolation level observed in various polymers.

Acknowledgements

The authors would like to acknowledge Arkema for financial support, the LEM laboratory (Arkema Serquigny) for facilitating

X-ray scattering experiments and SEM observations and the Carbon Nanotube and Nanomaterials Development Program at Groupement de Recherches de Lacq for the Graphistrength™ CNT samples.

References

[1] Thostenson ET, Ren Z, Chou TW. Composites Science and Technology 2001;6: 1899–912.
[2] Coleman JN, Khan U, Blau WJ, Gun'ko YK. Carbon 2006;44:1624–52.
[3] Andrews R, Weisenberger MC. Current Opinion in Solid State and Materials Science 2004;8:31–7.
[4] Du F, Fischer JE, Winey KI. Journal of Polymer Science, Part B: Polymer Physics 2003;41:3333–8.
[5] Jin Z, Pramoda KP, Goh SH, Xu G. Materials Research Bulletin 2002;37:271–8.
[6] Chen GX, Kim HS, Park BH, Yoon JS. Polymer 2006;47:4760–7.
[7] Liu T, Phang IY, Shen L, Chow SY, Zhang WD. Macromolecules 2004;37:7214–22.
[8] Pötschke P, Bhattacharyya AR, Janke A. European Polymer Journal 2004;40: 137–48.
[9] Qian D, Dickey EC, Andrews R, Rantell T. Applied Physics Letters 2000;76: 2868–70.
[10] Gao J, Zhao B, Itkis ME, Bekyarova E, Hu H, Kranak V, et al. Journal of the American Chemical Society 2006;128:7492–6.
[11] Xia H, Qiu G, Wang Q. Journal of Applied Polymer Science 2006;100:3123–30.
[12] Li J, Fang Z, Tong L, Gu A, Liu F. European Polymer Journal 2006;42:3230–5.
[13] Phang IY, Ma J, Shen L, Liu T, Zhang WD. Polymer International 2006;55:71–9.
[14] Li J, Fang Z, Tong L, Gu A, Liu F. Journal of Polymer Science, Part B: Polymer Physics 2006;44:1499–512.
[15] Schrauwen BAG, Govaert LE, Peters GWM, Meijer HEH. Macromolecular Symposia 2002;185:89–102.
[16] Schrauwen BAG, Breemen LCA, Spoelstra AB, Govaert LE, Peters GWM, Meijer HEH. Macromolecules 2004;37:8618–33.
[17] Corté L, Leibler L. Macromolecules 2007;40:5606–11.
[18] Corté L, Beaume F, Leibler L. Polymer 2005;46:2748–57.
[19] Muratoglu OK, Argon AS, Cohen RE. Polymer 1995;36:921–30.
[20] Dasari A, Yu ZZ, Mai YW. Macromolecules 2007;40:123–30.
[21] Sheng N, Boyce MC, Parks DM, Rutledge GC, Abes JI, Cohen RE. Polymer 2004; 45:487–506.
[22] Quan H, Li ZM, Yang MB, Huang R. Composites Sciences and Technology 2005; 65:999–1021.
[23] Shi HF, Zhao Y, Dong X, He CC, Wang DJ, Xu DF. Polymer International 2004; 53:1672–6.
[24] Kojima Y, Usuki A, Kawasumi M, Okada A, Kurauchi T, Kamigaito O, et al. Journal of Polymer Science, Part B: Polymer Physics 1994;32:625–30.
[25] Kim GM, Lee DH, Hoffmann B, Kressler J, Stöppelmann G. Polymer 2001;42:1095–100.
[26] Sandler J, Broza G, Nolte M, Schulte K, Lam YM, Shaffer MSP. Journal of Macromolecular Science, Part B: Physics 2003;42:479–88.
[27] Haggenmueller R, Fischer JE, Winey KI. Macromolecules 2006;39:2964–71.
[28] Li L, Li CY, Ni C, Rong L, Hsiao B. Polymer 2007;48:3452–60.
[29] Li L, Li CY, Ni C. Journal of the American Chemical Society 2005;128: 1692–9.
[30] Available from: www.graphistrength.com.
[31] Martinez-Salazar J, Cannom CG. Journal of Materials Science Letter 1984;3: 693–4.
[32] ImageJ is a public domain, Java-based image processing program developed at the National Institutes of Health, http://rsb.info.nih.gov/ij/download.html.
[33] Koham MI. Nylon plastics handbook. Hanser Publishers; 1995.
[34] Bhattacharyya AR, Sreekumar TV, Liu T, Kumar S, Ericson LM, Hauge RH, et al. Polymer 2003;44:2373–7.
[35] Sano M, Sasaki DY, Kunitake T. Science 1992;258:441–3.